Design and Kinematic Analysis on a Novel Serial-Parallel Hybrid Leg for Quadruped Robot

Jianzhuang Zhao[1,2], Kai Liu[1,2], Fei Zhao[1,2(✉)], and Zheng Sun[1,2]

[1] Shaanxi Key Laboratory of Intelligent Robots, Xi'an Jiaotong University, Xi'an 710094, Shaanxi, People's Republic of China
ztzhao@xjtu.edu.cn

[2] School of Mechanical Engineering, Xi'an Jiaotong University, Xi'an 710094, Shaanxi, People's Republic of China

Abstract. Aiming to improve the performances and reduce the manufacturing cost of the current legs for quadruped robots, this paper presents a novel 3 DOF serial-parallel hybrid leg. We design a prototype 3D model and give the analytical expressions of inverse and forward kinematics. End-effector workspace is computed using the numerical forward kinematics. The analysis and calculations show that this hybrid leg with simple structure combines the advantages of both serial and parallel mechanisms: high stiffness, high bearing capacity, low structural inertia and large workspace. This research has great significance to a series of further studies on dynamic analysis, mechanism optimal and system control of this novel hybrid leg.

Keywords: Quadruped robot · Serial-parallel hybrid leg · Kinematic analysis · Co-simulation

1 Introduction and Related Works

Quadruped robot is an essential part of robotics and has become a research hotspot in the past decade (Ananthanarayanan et al. 2012), since this kind of robots can complete a lot of difficult works in dangerous and complex environments instead of human, such as disaster relief, minesweeping, environmental detection etc. (Gehring et al. 2016). One of the most important components of quadruped robot is the leg which determines the motion performance (Seok et al. 2015).

Most structures of legs for current quadruped robot are serial such as BigDog (Ding et al. 2015) from Boston Dynamic company. HyQ robot (Semini et al. 2011) was developed by Italy and Shandong University designed Scalf robot (Chai et al. 2014). These serial structures have large workspace, but the stiffness and bearing capacity are low. On the other hand, walking robot with parallel leg was raised by Rong et al. (2012). WL-15, WL-16RIV (Sugahara et al. 2005)

H. Yu et al. (Eds.): ICIRA 2019, LNAI 11742, pp. 436–447, 2019.
https://doi.org/10.1007/978-3-030-27535-8_39

was proposed by Waseda University and Minitaur (Kenneally et al. 2016) was designed by University of Pennsylvania. These parallel structure legs with complex structure and small workspace have high stiffness, high bearing capacity, high stability and low weight-load ratio. In order to combine the advantages of the two structures, Xinghua et al. summarized the characteristics of these legs' configurations of current quadruped robots, and proposed three different hybrid leg structures (Xianbao and Chenkun 2013). Gao et al. proposed a new 4-DOF hybrid leg and solved the kinematics problems (Gao et al. 2015). These hybrid legs showed the expected performance and achieved good effects in practical applications. While, some of these hybrid legs used complex spatial structures which are difficult to manufacture and the costs are high.

To overcome the limitations of serial and parallel structures, and reduce manufacturing costs of current serial-parallel hybrid legs, we propose a novel and simplified serial-parallel hybrid leg, which is composed of two planar mechanisms in this paper. The paper is organized as follows. The mechanical design of the hybrid leg is introduced firstly. Section 3 analyze the degrees-of-freedom (DOF) of this novel structure and design a prototype. In Sect. 4, we report the details of this hybrid leg kinematics. Workspace analysis and verification results are presented in Sect. 5. Our conclusions and future work are discussed in Sect. 6.

2 Overview of Mechanical Design

The schematic diagram of the proposed serial-parallel leg is shown in Fig. 1, including the frame 1, the links 2A, 2B, 3A, 3B, 4A and 4B, the rotating shafts 5, the thigh link 6, the hip joint 7, the thigh 8 and the calf 9. The geometrical parameters of (N)A and (N)B are same.

This serial-parallel mechanism is composed of one parallel part and one serial part. The overall spatial mechanism can be disassembled into two planar mechanisms to simplify the kinematic analysis. And the following sections are based on this method. The parallel portion is horizontally connected the frame 1 by the links 2A, 2B. And the links 2A, 2B are fixed with frame 1. The serial section is vertical. The two portions are connected through the thigh link 6, and all the motion pairs in the entire mechanism are rotating pairs.

3 Analysis of DOF and Prototype Design

The separated two parts are shown in Fig. 2. Firstly, for the serial portion, the open-loop four-link mechanism consists of the frame 1, the hip joint 7, the thigh 8 and the calf 9. The frame 1 is fixed with no DOF, and the remaining three members are free. Connected by three rotating pairs, this structure has no virtual constraints and local DOF. Above all, the DOF of the serial portion can be written by Kutzbach-Grübler(KG) formula as follows:

$$f_1 = 3n - (2p_l + p_h) = 3 \times 3 - (2 \times 3) = 3 \tag{1}$$

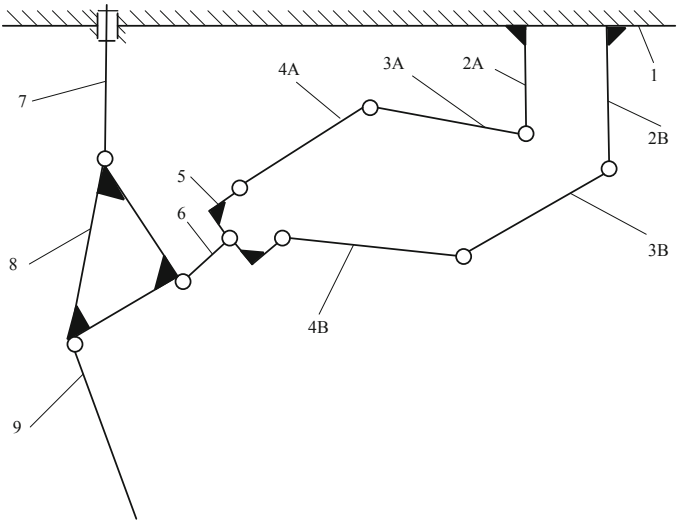

Fig. 1. Schematic diagram of whole structure.

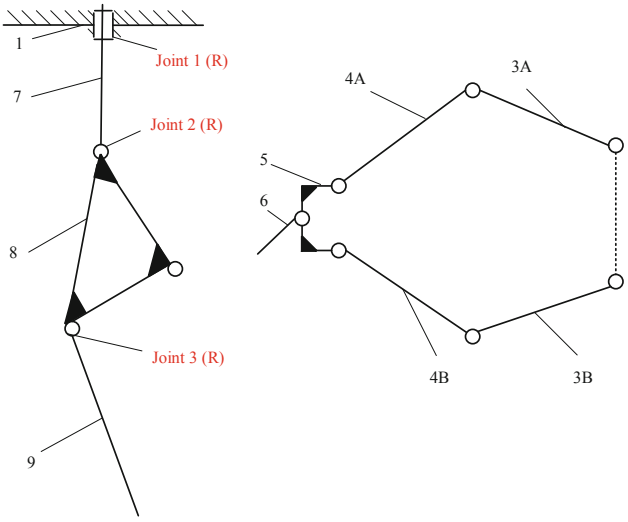

Fig. 2. Separated serial and parallel parts.

where f_1 is the DOF of serial part, n is the number of links, p_l is the number of lower pair and p_h is the number of higher pair. Then, for the DOF of the parallel portion, this portion can be simplified as a plane-symmetric six-link mechanism with external constraint. The rotating shafts 5 is indirectly connected to the frame 1 through the thigh link 6 and the serial part. It is externally constrained, losing one DOF. Therefore, the DOF of the parallel portion is:

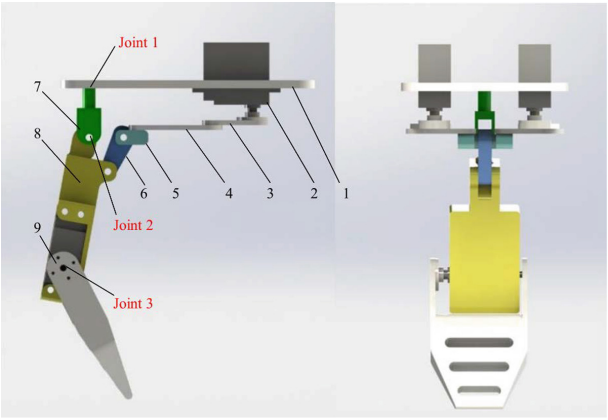

Fig. 3. 3D model of the novel parallel-serial hybrid leg.

$$f_2 = 3n - (2p_l + p_h) = 3 \times 4 + 2 - (2 \times 6) = 2 \tag{2}$$

where f_2 is the DOF of parallel part.

For the whole structure, it should be note that the hip joint 7 and the thigh 8 are driven by the parallel portion through the thigh link 6. They are not independent components. Only the rotation of the knee between the thigh 8 and the calf 9 is independent in serial portion. So, there are 3 DOF for the entire parallel-serial leg, 2 DOF in the parallel portion, and 1 DOF in the serial part, respectively.

From the above analysis, we design the links 3A, 3B driven by two servo motors and another motor is used for the thigh 8 at the joint 3 to drive the calf 9. The 3D model designed by Solidworks is shown in Fig. 3 where 2, 3 and 4 represent the links 2(A, B), 3(A, B) and 4(A, B). And, the three joints of the serial part is also marked in Fig. 3.

It can be easily found that there are two servo motors fixed in the frame 1 compared with the traditional 3-DOF serial leg in which only one motor is fixed in the base. Moreover, three chains from the end of the calf 9 to the frame 1 can be found in this hybrid leg. Therefore, this novel hybrid leg has the advantages of high stiffness, high bearing capacity and low weight-load ratio. At the same time, this design reduces the inertia when the robot lifts the leg, which improves the efficiency and the flexibility of this leg. Last but not least, all components of this hybrid leg can be easily made, and the cost is lower.

4 Kinematic Analysis

4.1 Modified D-H Model

The kinematic model is critical for solving the inverse and forward kinematics. We define the positive axes direction as counterclockwise rotation. The schematic of the frames of serial part is shown in Fig. 4.

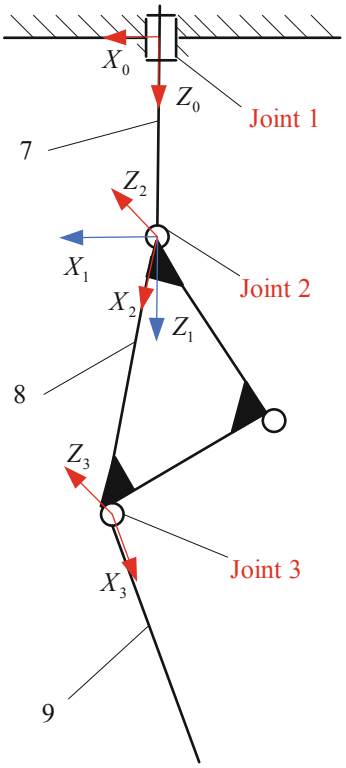

Fig. 4. Frames of serial part.

Based on this model and given the range of the joint angles, the following modified D-H parameters of the serial part were determined in Table 1.

Table 1. Modified D-H parameters of serial part.

i	a_{i-1}	α_{i-1}	d_i	θ_i	Range of θ_i
1	0	0°	d_1	θ_1	$[-40°, 40°]$
2	0	−90°	0	θ_2	$[-140°, -75°]$
3	a_2	0°	0	θ_3	$[-90°, 90°]$

For the modified D-H parameters, the general homogeneous transformation matrix ${}_{i}^{i-1}T$ can be written as:

$$ {}_{i}^{i-1}T = \begin{bmatrix} c\theta_i & -s\theta_i & 0 & 0 \\ s\theta_i c\alpha_{i-1} & c\theta_i c\alpha_{i-1} & -s\alpha_{i-1} & -d_i s\theta_i \\ s\theta_i s\alpha_{i-1} & c\theta_i s\alpha_{i-1} & -s\alpha_{i-1} & d_i c\alpha_{i-1} \\ 0 & 0 & 0 & 1 \end{bmatrix} \tag{3} $$

where $c\theta_i = cos\theta_i$, $s\theta_i = sin\theta_i$, $c\alpha_{i-1} = cos\alpha_{i-1}$, $s\alpha_{i-1} = sin\alpha_{i-1}$.

Bring the parameters from Table 1 into formula 3, the ${}^0_1T$, ${}^1_2T$, ${}^3_2T$ can be obtained. Since the axes of joint 2 and joint 3 are parallel, ${}^1_3T$ calculated first using ${}^1_3T = {}^1_2T{}^2_3T$. Finally, by ${}^0_3T = {}^0_1T{}^1_3T$, the complete transformation matrix ${}^0_3T$ can be got.

$$ {}^0_3T = {}^0_1T{}^1_3T = \begin{bmatrix} c_1c_{23} & -c_1s_{23} & -s_1 & a_2s_{23} \\ s\theta_ic\alpha_{i-1} & c\theta_ic\alpha_{i-1} & -s\alpha_{i-1} & -d_is\theta_i \\ s\theta_is\alpha_{i-1} & c\theta_is\alpha_{i-1} & -s\alpha_{i-1} & d_ic\alpha_{i-1} \\ 0 & 0 & 0 & 1 \end{bmatrix} \tag{4} $$

where $c_1 = cos\theta_1$, $s_1 = sin\theta_1$, $c_{23} = cos(\theta_2 + \theta_3)$, $s_{23} = sin(\theta_2 + \theta_3)$.

4.2 Inverse Kinematics

The inverse kinematics computation of this hybrid leg includes the following two steps:

(a) Inverse solution of workspace to joint space.
(b) Inverse solution of joint space to driving space.

Inverse Solution of Workspace to Joint Space. The equation of motion for the serial part can be written as:

$$ {}^0_3T = \begin{bmatrix} n_x & o_x & a_x & p_x \\ n_y & o_y & a_y & p_y \\ n_z & o_z & a_z & p_z \\ 0 & 0 & 0 & 1 \end{bmatrix} = {}^0_1T(\theta_1){}^1_2T(\theta_1){}^2_3T(\theta_3) \tag{5} $$

The idea of the inverse solution of the workspace to the joint space is that we know the configuration of the end effector (foot ending) to find the joint angles θ_1, θ_2, θ_3. Multiplying ${}^0_1T^{-1}(\theta_1)$ on the left of the two sides of Eq. 5, we can get the Eq. 6. The elements (2, 4) of the two matrixes are equal and the equation $-s_1p_x + c_1p_y = 0$ can be obtained. So, the expression of θ_1 is: $\theta_1 = arctan(p_y/p_x)$.

$$ \begin{bmatrix} c_1 & s_1 & 0 & 0 \\ -s_1 & c_1 & 0 & 0 \\ 0 & 0 & 1 & -d_1 \\ 0 & 0 & 0 & 1 \end{bmatrix} \begin{bmatrix} n_x & o_x & a_x & p_x \\ n_y & o_y & a_y & p_y \\ n_z & o_z & a_z & p_z \\ 0 & 0 & 0 & 1 \end{bmatrix} = {}^1_2T(\theta_2){}^2_3T(\theta_3) = {}^1_3T(\theta_2, \theta_3) \tag{6} $$

Then, make the elements (1, 4) and (3, 4) of the two matrixes are equal, the expression of θ_2 can be written as:

$$ \begin{cases} p_xc_1 + p_ys_1 = a_2c_2 \\ p_z - d_1 = -a_2s_2 \end{cases} \rightarrow \theta_2 = arctan[(d_1 - p_z)/(p_xc_1 + p_ys_1)] \tag{7} $$

Next, multiplying ${}^1_2T^{-1}(\theta_2)$ on the left of the two sides of Eq. 6. The elements (1, 1) and (2, 1) of the two matrixes are equal. We can get the following equation: $\theta_3 = arctan[-(n_xc_1s_2 + n_ys_1s_2 + n_zc_2)/(n_xc_1c_2 + n_ys_1c_2 - n_zs_2)]$.

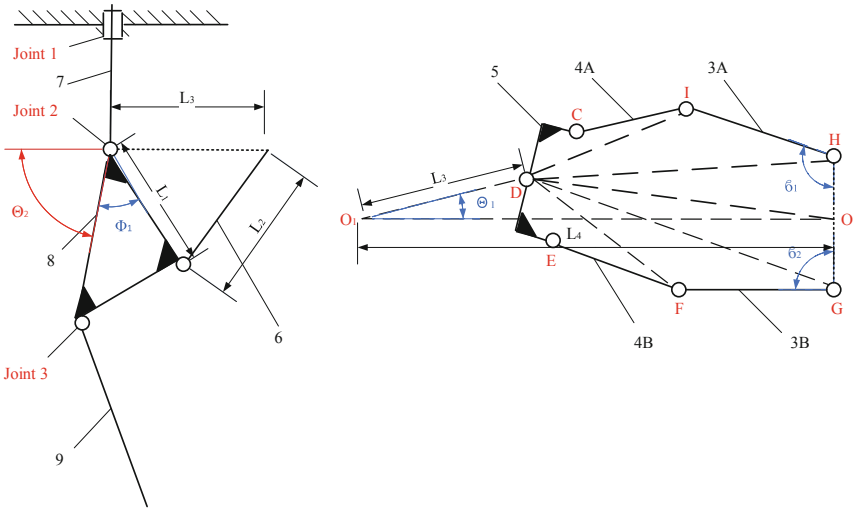

Fig. 5. Sketch of inverse kinematics.

Finally, the inverse kinematic solution from the workspace to joint space is shown in Eq. 8.

$$\begin{cases} \theta_1 = arctan(p_y/p_x) \\ \theta_2 = arctan[(d_1 - p_z)/(p_x c_1 + p_y s_1)] \\ \theta_3 = arctan[-(n_x c_1 s_2 + n_y s_1 s_2 + n_z c_2)/(n_x c_1 c_2 + n_y s_1 c_2 - n_z s_2)] \end{cases} \tag{8}$$

Inverse Solution of Joint Space to Driving Space. In this step, geometric constraints are used to find the relationship between the joint angles θ_1, θ_2 and the driving angles β_1, β_2. Because the range of θ_1 is symmetrical, we can only focus on half of it.

The inverse solution structure sketch of the two parts is shown is shown in Fig. 5. The motion of serial part in the vertical plane is analyzed firstly. In Fig. 5, assuming L_1, ϕ_1 and L_2 are known of the $\triangle(L_1 L_2 L_3)$, the length of L_3 can be solved by the cosine theorem which is:

$$L_3 = L_1 cos(\theta_2 - \phi_1) + \sqrt{[2L_1 cos(\theta_2 - \phi_1)]^2 - 4[(L_1)^2 - (L_2)^2]}/2 \tag{9}$$

In order to make the following calculations of parallel part concise, we named the links and angles as follows: $CD = DE = L_5$, $CI = EF = L_6$, $IH = FG = L_7$, $HO = OG = L_8$, $DO = L_9$, $DH = L_{10}$, $DI = L_{11}$, $DG = L_{12}$, $DF = L_{13}$; $\angle O_1OD = \phi_2$, $\angle OHD = \phi_3$, $\angle HDI = \phi_4$, $\angle CDI = \phi_5$, $\angle DHI = \phi_6$, $\angle FDG = \phi_7$, $\angle EDF = \phi_8$, $\angle DGO = \phi_9$, $\angle DGF = \phi_{10}$.

In $\triangle O_1OD$, L_9 can be known by cosine theorem and ϕ_2 can be known by sine theorem which can be written as:

$$\begin{cases} L_9 = \sqrt{(L_3)^2 + (L_4)^2 - 2L_3L_4cos\theta_1} \\ \phi_2 = arcsin(L_3sin\theta_1/L_9) \end{cases} \tag{10}$$

Then, the $\angle O_1DO$ and $\angle DOH$ can be written as:

$$\begin{cases} \angle O_1DO = \pi - \theta_1 - \phi_2 \\ \angle DOH = \pi/2 - \phi_2 \end{cases} \tag{11}$$

After that, ϕ_3 can be found in $\triangle HOD$ using the same method in $\triangle O_1OD$ which is:

$$\phi_3 = arcsin[L_9sin(\pi/2 - \phi_2)/L_{10}] \tag{12}$$

At the same time, $\angle ODH$ and $\angle CDI$ can be written as:

$$\begin{cases} \angle ODH = \pi/2 + \phi_2 - \phi_3 \\ \angle CDI = \phi_5 = \theta_1 + \phi_3 - \phi_4 \end{cases} \tag{13}$$

Next, regard L_{11} as an unknown parameter, ϕ_4 and L_{11} can be known using the cosine theorem in $\angle CID$ and $\angle HID$ which can be written as:

$$\begin{cases} \phi_5 = \theta_1 + \phi_3 - \phi_4 \\ L_{11} = L_{10}cos\phi_4 - \sqrt{(2L_{10}cos\phi_4)^2 - 4[(L_{10})^2 - (L_7)^2]}/2 \\ L_{11} = L_5cos\phi_5 - \sqrt{(2L_5cos\phi_5)^2 - 4[(L_5)^2 - (L_6)^2]}/2 \end{cases} \rightarrow \phi_4 \rightarrow L_{11} \tag{14}$$

So, ϕ_6 can be known by:

$$\phi_6 = arcsin(L_{11}sin\phi_4/L_7) \tag{15}$$

Because the parallel part is symmetrical, ϕ_9 and ϕ_{10} can be obtained by same process, which can be written as:

$$\phi_9 = arcsin[L_9sin(\pi/2 + \phi_2)/L_{12}]; \phi_{10} = arcsin(L_{13}sin\phi_7/L_7) \tag{16}$$

Finally, the expressions of β_1, β_2 can be written as:

$$\begin{cases} \beta_1 = \phi_3 + \phi_6 = arcsin[L_9sin(\pi/2 - \phi_2)/L_{10}] + arcsin(L_{11}sin\phi_4/L_7) \\ \beta_2 = \phi_9 + \phi_{10} = arcsin[L_9sin(\pi/2 + \phi_2)/L_{12}] + arcsin(L_{13}sin\phi_7/L_7) \end{cases} \tag{17}$$

What needs to be explained here is that the Eq. 17 gives the relationship between joint angles (θ_1, θ_2) and the driving angles (β_1, β_2). Therefore, in the forward kinematics part, we only focus on the serial part.

4.3 Forward Kinematics

The forward kinematic problem is that the joint angles are already given to find the expression of the end of this hybrid leg in frame 0. In this paper, we regard

the central point P which is at the end of calf 9 as the end of this leg. So, θ_1, θ_2, θ_3 is known and the expression of point P in frame 3 is $P_3 = (x_3, y_3, z_3)$.

Above all, it is easy to solve the forward kinematic problem using homogeneous transformation matrix ${}^0_3T$, which can be written as:

$$P_0 = \begin{bmatrix} x_0 \\ y_0 \\ z_0 \\ 1 \end{bmatrix} = {}^0_3TP_3 = \begin{bmatrix} c_1c_{23} & -c_1s_{23} & -s_1 & a_2s_{23} \\ s\theta_i c\alpha_{i-1} & c\theta_i c\alpha_{i-1} & -s\alpha_{i-1} & -d_i s\theta_i \\ s\theta_i s\alpha_{i-1} & c\theta_i s\alpha_{i-1} & -s\alpha_{i-1} & d_i c\alpha_{i-1} \\ 0 & 0 & 0 & 1 \end{bmatrix} \begin{bmatrix} x_3 \\ y_3 \\ z_3 \\ 1 \end{bmatrix} \tag{18}$$

where $P_0 = (x_0, y_0, z_0)$ is the position of point P in frame 0. When the joint angle is given, the P_0 can be uniquely determined.

5 Workspace Analysis and Verification

5.1 Workspace Analysis

The workspace of the mechanism refers to the position that the end effector or reference point of the mechanism can reach. It is an important indicator to measure the performance of the robot. For this structure, we chose point P as the reference point. And the geometric parameters of the 3D model designed before were given in Table 2. a_3 is the length of the calf 9.

Table 2. The geometric parameters of serial part.

Name	d_1	a_2	a_3
Length/(mm)	35	81.27	90

Bring the joint angles into the forward kinematic Eq. 18, the workspace of this hybrid leg can be plotted by Matlab which is shown in Fig. 6. From the result, we found the workspace looks like a mushroom and the $z_0max = 206.27$ mm. It is clearly that the workspace of this hybrid leg is larger than the traditional 3-DOF parallel robot with same geometric parameters.

5.2 Verification

The 3D model of the hybrid leg designed by Soildworks was imported into Adams to verify the results of our analysis. In Adams, the complete constraints were added to this leg and the result is in Fig. 7(a) shows that the DOF of this structure is 3, which is consistent with the DOF analysis before. We planned a backwards movement in the workspace for this structure which lasts 25 s and the foot movement track is:

$$\begin{cases} x_0 = -t \\ y_0 = 0 \\ z_0 = 206.27 - t \end{cases} \tag{19}$$

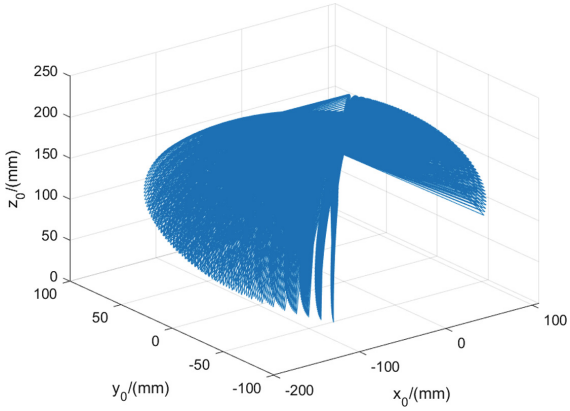

Fig. 6. Workspace of this hybrid leg.

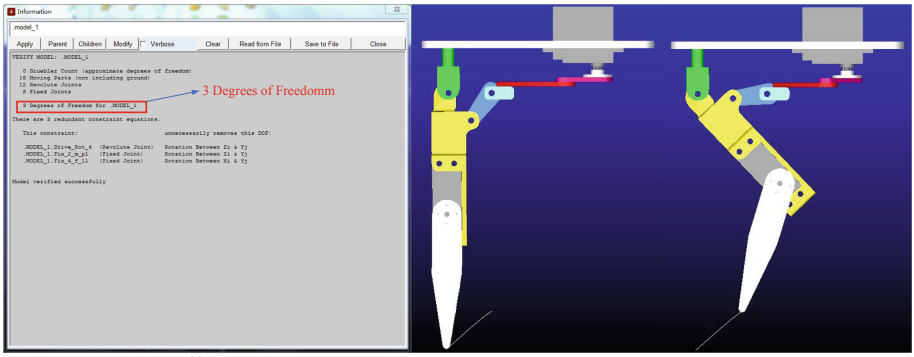

Fig. 7. Adams simulation.

Next, the result of inverse kinematics calculated by Matlab was imported into Adams to drive this leg. The beginning and end of the simulation positions were shown in Fig. 7(b).

From the equation of the track, the joint angles $(\theta_1, \theta_2, \theta_3)$ and the driving angles $(\beta_1, \beta_2, \beta_3)$ can be obtained by inverse kinematics, which the $\theta_1 = 0, \beta_1 = \beta_2$ in this track. So, we just needed to focus on $(\beta_1, \theta_2, \theta_3)$. The simulation results of $(\beta_1, \theta_2, \theta_3)$ were shown in Fig. 8. The green full curve represented the results calculated by Matlab and the red dummy curve was the results from Adams. And, it was easy to find that the angles $(\beta_1, \theta_2, \theta_3)$ in Fig. 8 were almost identical.

For the forward kinematic, we chose the point when $t = 10\,\mathrm{s}$ to prove the correctness. At this point, $\theta_1 = 0°, \theta_2 = -113.96°, \theta_3 = 38.77°$ and$x_0 = -10, y_0 = 0, z_0 = 196.27$ by Eq. (19). Bring the joint angles into Eq. (18), the position of $\hat{P}$ was: $\hat{x}_0 = -9.998$, $\hat{y}_0 = 0$, $\hat{z}_0 = 196.277$ which was almost the same with (x_0, y_0, z_0).

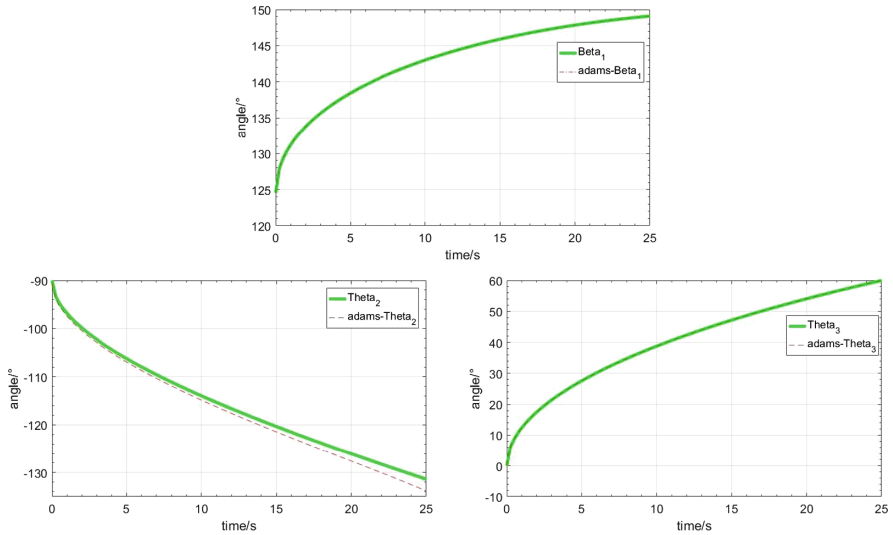

Fig. 8. Co-simulation results. (Color figure online)

Above all, our kinematic analysis was right proved by the co-simulation with Matlab and Adams.

6 Conclusion and Future Work

As an essential component of quadruped robots, a novel serial-parallel hybrid leg is proposed to improve the motion performances. The DOF of this novel structure is 3 which is proved later. A prototype 3D model is designed, and analytical equations of inverse and forward kinematics are derived. The workspace for this hybrid leg is also plotted. By Matlab and Adams co-simulation, the analysis is verified. These analysis results show that this hybrid leg combines the advantages of both serial and parallel mechanisms: high stiffness, high bearing capacity, low structural inertia and large workspace. The manufacturing cost of this hybrid leg is low, which means it is easy to be popularized and applied.

The future work includes velocity analysis, dynamic analysis and kinematic parameter optimization to realize the desired motion-force relationship. A prototype hardware should be implemented and experimental verified.

Acknowledgment. This research is supported by the national key development plan project of intelligent robot (No. 2018YFB4505), ministry of science and technology of China.

References

Ananthanarayanan, A., Azadi, M., Kim, S.: Towards a bio-inspired leg design for high-speed running. Bioinspir. Biomim. **7**(4), 046,005 (2012)

Chai, H., Meng, J., Rong, X., Li, Y.: Design and implementation of scalf, an advanced hydraulic quadruped robot. Robot **36**(4), 385–391 (2014)

Ding, L., Wang, R., Feng, H.: Key technology analysis of bigdog quadruped robot. J. Mech. Eng. **51**(7), 1–23 (2015)

Gao, J., Li, M., Hou, B., Wang, B.: Kinematics analysis on the serial-parallel leg of a novel quadruped walking robot. Opt. Precis. Eng. **23**(11), 3147–3160 (2015)

Gehring, C., et al.: Practice makes perfect: an optimization-based approach to controlling agile motions for a quadruped robot. IEEE Robot. Autom. Mag. **23**(1), 34–43 (2016)

Kenneally, G., De, A., Koditschek, D.E.: Design principles for a family of direct-drive legged robots. IEEE Robot. Autom. Lett. **1**(2), 900–907 (2016)

Rong, Y., Jin, Z.L., Qu, M.K.: Design of parallel mechanical leg of six-legged robot. Guangxue Jingmi Gongcheng (Opt. Precis. Eng.) **20**(7), 1532–1541 (2012)

Semini, C., Tsagarakis, N.G., Guglielmino, E., Focchi, M., Cannella, F., Caldwell, D.G.: Design of HyQ-a hydraulically and electrically actuated quadruped robot. Proc. Inst. Mech. Eng. Part I: J. Syst. Control Eng. **225**(6), 831–849 (2011)

Seok, S., et al.: Design principles for energy-efficient legged locomotion and implementation on the mit cheetah robot. IEEE/ASME Trans. Mechatron. **20**(3), 1117–1129 (2015)

Sugahara, Y., et al.: Walking control method of biped locomotors on inclined plane. In: Proceedings of the 2005 IEEE International Conference on Robotics and Automation, pp. 1977–1982. IEEE (2005)

Xianbao, T.X.G.F.C., Chenkun, Q.: Mechanism design and comparison for quadruped robot with parallel-serial leg. J. Mech. Eng. **6** (2013)